Molecular Dynamics Simulation of Atactic Polystyrene. 1. Comparison with X-ray Scattering Data

M. Mondello,† Hyung-Jin Yang,‡ Hidemine Furuya,§ and Ryong-Joon Roe*

Department of Materials Science and Engineering, University of Cincinnati, Cincinnati, Ohio 45221

Received February 9, 1994; Revised Manuscript Received April 1, 1994®

ABSTRACT: A molecular dynamics simulation of bulk atactic polystyrene was performed. A united atom model and an all atom model were developed, in both of which the bond lengths were held fixed and the phenyl group was represented by a rigid, planar hexagon. The degree of success of the simulation was examined by comparing the calculated X-ray scattering intensity curve with experiment. The united atom model reproduces the so-called "polymerization peak", and the calculated curve agrees well with one of the most recently published experimental data. The degree of agreement achieved is in fact comparable to the degree to which two published experimental curves agree with each other. The agreement in the radial distribution function between the calculated and experimentally derived one is good in the r range smaller than 9 Å but deteriorates somewhat for larger r. There are again uncertainties in the experimental radial distribution function itself at large distances, however, as can be seen by comparing experimental curves obtained by two different groups. In contrast to the united atom model, the all atom model was found to give a result which clearly disagrees with experimental results, and one of the commercially available software gave an even worse result. The nature of smearing that accrues in the experimentally determined radial distribution function, as a consequence of the differing q dependencies of C and H atomic scattering factors and the limited q range accessible to experiment, has been examined by calculating the radial distribution function directly from the simulation result.

Introduction

Understanding the structure of amorphous polymers is a challenging task. Traditionally one of the principal techniques employed for this purpose has been the X-ray diffraction method. Structural information is obtained either by studying the radial distribution function derived from the intensity data or by comparing the scattering curves with theoretical ones calculated from model structures. Recently[1,2] the technique of computer simulation has emerged as a powerful new technique for studying static and dynamic properties of bulk amorphous polymers. Analysis of the atomic coordinates obtained from the simulation can potentially allow evaluation of the short-range structure in much greater detail than any experimental methods can. The usefulness of this approach depends critically on the success of the model to simulate the real polymer faithfully. We have now applied the molecular dynamics simulation technique[3] to model a glassy atactic polystyrene of realistic bulk density. In this paper we examined the degree of our success by comparing the calculated results with those obtained from experimental X-ray diffraction studies. The results of analysis of the structure itself will be presented in a later publication.

Atactic polystyrene is probably the most widely studied among all amorphous polymers. In addition to the large number of experimental data available, molecular modeling techniques have also been applied recently[4,5] to the study of this polymer. Yet many questions still remain about the way the atoms, segments, and chains are packed into a dense, glassy structure. X-ray diffraction study of polystyrene was made as early as 1927 by Katz[6] and since then a succession of workers[7-17] have repeatedly applied the technique to this polymer. One of the features that have attracted a particular interest is the presence of the so-called "polymerization peak" (or "polymerization ring")[6,7] in the diffraction pattern at q ($=4\pi \sin\theta/\lambda$) equal to about 0.75 Å^{-1} in addition to the main amorphous "halo" at q = 1.3 Å^{-1}. Theoretical curves[12,16] based on models of an isolated, disordered chain have all failed to reproduce this polymerization ring. This is consistent with the generally held belief that the polymerization ring arises from an *inter*molecular interference effect. Clearly, an understanding of the polymerization ring would require a model that accounts not only for the conformational characteristics of individual chains but also the interactions between nonbonded atoms and segments. The molecular dynamics simulation technique is well suited for this purpose.

In this work we pay attention to producing a program that is computationally efficient. A good efficiency is particularly important for polystyrene, which has a relatively high T_g and consequently a slow relaxation rate. For this purpose we adopt the united atom approximation, in which the hydrogen atoms are combined to the carbon atoms to which they are attached. This reduces the number density of atoms to a half and the average number of neighbor pairs within a given distance to a quarter. Since 70–80% of computational time is spent in calculating the nonbonded neighbor interactions, the resulting overall gain in computation speed is by at least a factor of 3. Such an increased efficiency is useful of course only if the united approximation does not introduce any undesirable effects into the model. To check the possibility of such artifacts that might arise from the approximation, we have also developed a program based on an all atom model. To our surprise, the all atom model produces results that agree less well with experiment than the united atom model does, as will be described below. As another means of increasing the efficiency, we have chosen to have the carbon–carbon bonds constrained to fixed lengths instead of undergoing springlike vibrations. Eliminating the bond length stretching, which is normally the fastest among

† Present address: Exxon Research and Engineering Co., Annandale, NJ 08801.
‡ Present address: Department of Physics, Jochiwon Campus, Korea University, Korea.
§ Present address: Department of Polymer Chemistry, Tokyo Institute of Technology, Meguro-ku, Tokyo, Japan.
® Abstract published in *Advance ACS Abstracts*, May 15, 1994.

0024-9297/94/2227-3566$04.50/0

Table 1. Force Field Parameters for the United Atom Model

1. Nonbonded Interaction

$V_{nb} = \epsilon[(r_0/r)^{12} - 2(r_0/r)^6]$; $\epsilon = (\epsilon_1\epsilon_2)^{0.5}$; $r_0 = (r_1 + r_2)/2$

ϵ_1 = 0.12 kcal/mol r_1 = 4.321 Å for CH_2

ϵ_1 = 0.09 kcal/mol r_1 = 4.153 Å for aliphatic CH

ϵ_1 = 0.12 kcal/mol r_1 = 4.153 Å for aromatic C and CH

cutoff distance: 7.65 Å

2. Bond Length

1.53 Å for aliphatic CH_2–CH

1.51 Å for CH(aliph)–C(arom)

1.40 Å between two aromatic C atoms

(1.10 Å for C–H, used for the calculation of X-ray and neutron-scattering intensities)

3. Bond Angle

$V_\theta = k_\theta(\theta - \theta_0)^2$

k_θ = 60 kcal/mol θ_0 = 109.5° for aliphatic CH_2–CH–CH_2

k_θ = 63 kcal/mol θ_0 = 109.5° for aliphatic CH–CH_2–CH

k_θ = 60 kcal/mol

θ_0 = 109.5° for CH_2(aliph)– CH(aliph)–C(arom)

k_θ = 70 kcal/mol

θ_0 = 120.0° for CH(aliph)–C(arom)–CH(arom)

4. Torsion for X–CH(aliph)–CH_2(aliph)–X

$V_\phi = k_\phi(1 - \cos 3\phi)$

k_ϕ = 1.4 kcal/mol

5. Phenyl Ring Torsion around CH(aliph)–C(arom)

$V_\chi = k_\chi \cos^2(\chi - \chi_0)$

k_χ = 2 kcal/mol χ_0 = 90°

6. Phenyl Ring (Out-of-Plane) Bending

$V_\psi = k_\psi\psi^2$

k_ψ = 80 kcal/mol

7. Improper Torsion

(To Maintain the Stereochemical Configuration of Aliphatic CH)

$V_\omega = k_\omega\omega^2$

k_ω = 50 kcal/mol (for the definition of ω, see text)

modes of motions in the system, allows the use of a larger time step in the integration of the equations of motion. According to a study by van Gunsteren and Karplus,[18] the use of fixed bond lengths does not influence the dynamics on a time scale longer than 0.05 ps, in contrast to fixed bond angles that modify the dynamics significantly. We further constrain the six carbon atoms in the phenyl group to remain in a planar hexagonal configuration by using the algorithm suggested by Ciccotti et al.[19,20] Such a constrained geometry algorithm was used for a molecular dynamics (MD) simulation of liquid benzene[21] that gave a local structure in good agreement with experimental data.

Models and Computational Method

The model consists of a single polystyrene molecule having 80 monomer units and its images generated by the periodic boundary conditions. The cubic MD cell therefore contains 640 carbon atoms in the case of the united atom model and 640 carbon and 640 hydrogen atoms in the case of the all atom model. The size of the cell was adjusted to have the density match the experimental one; for example, the density of 1.028 g/cm^3 is attained by having a cell of edge length equal to 2.38 nm. The stereochemical sequence of the styrene units along the chain was generated according to the Bernoulli statistics with the expectation value of meso dyads equal to 0.40, the value found with experimental atactic polystyrene.[22]

The force field parameters employed are listed in Tables 1 and 2. The parameters for the united atom model were mostly taken from the united atom AMBER force field published by Weiner et al.[23] The parameters for the all atom model were taken similarly from the all atom AMBER force field published by Weiner et al.[24] No electrostatic or π-electron interactions were included. For the torsion along the C–C bonds in the chain backbone we

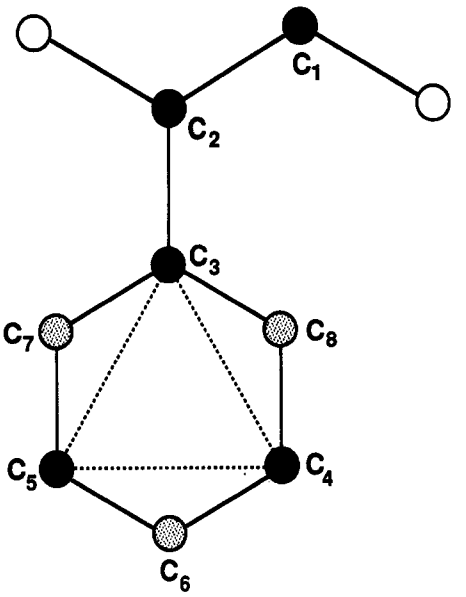

Figure 1. Numbering of carbon atoms in the styrene unit.

Table 2. Force-Field Parameters for the All Atom Model

1. Nonbonded Interaction

$V_{nb} = \epsilon[(r_0/r)^{12} - 2(r_0/r)^6]$; $\epsilon = (\epsilon_1\epsilon_2)^{0.5}$; $r_0 = (r_1 + r_2)/2$

ϵ_1 = 0.06 kcal/mol r_1 = 3.60 Å for aliphatic C

ϵ_1 = 0.12 kcal/mol r_1 = 3.70 Å for aromatic C

ϵ_1 = 0.01 kcal/mol r_1 = 3.08 Å for H

cutoff distance 7.65 Å

2. Bond Length

1.526 Å for aliphatic C–C

1.510 Å for C(aliph)–C(arom)

1.400 Å between two aromatic C atoms

1.090 Å for C–H

3. Bond Angle

$V_\theta = k_\theta(\theta - \theta_0)^2$

k_θ = 40 kcal/mol θ_0 = 109.5° for aliphatic C–C–C

k_θ = 35 kcal/mol θ_0 = 109.5° for aliphatic C–C–H

k_θ = 36 kcal/mol θ_0 = 109.5° for aliphatic H–C–H

k_b = 63 kcal/mol θ_0 = 114.0° for C(aliph)–C(aliph)–C(arom)

k_b = 35 kcal/mol θ_0 = 109.5° for H–C(aliph)–C(arom)

k_b = 70 kcal/mol θ_0 = 120.0° for C(aliph)–C(arom)–C(arom)

4. Torsion

$V_\phi = k_\phi(1 - \cos 3\phi)$

k_ϕ = 1.3 kcal/mol

5. Phenyl Ring (Out-of-Plane) Bending

$V_\psi = k\psi\psi^2$

k_ψ = 80 kcal/mol

applied a 3-fold intrinsic potential, allowing the difference between the trans and gauche states to develop through the further, nonbonded interactions operating between atoms three or more bonds apart.

As has been discussed by Flory and co-workers[25,27] and by Tonelli,[26] the torsional rotation of the phenyl group around the C_2–C_3 bond joining the phenyl group to the backbone (see Figure 1 for numbering of atoms) is severely restricted as a result of steric hindrances between the ortho CH on the phenyl group and the aliphatic hydrogens. In the absence of hydrogens in the united atom model the corresponding steric hindrances are greatly reduced, and therefore to simulate the restricted rotation an additional 2-fold torsional potential was imposed on the rotation around the C_2–C_3 bond, as indicated in Table 1.

In the united atom model, if the sp^3 stereochemical configuration of the bonds around C_2 is to be maintained, we must prevent the collapse of the four carbons, C_1, C_3, C_1', and C_2, on to a plane. To accomplish this, many different ad hoc potentials, often referred to as improper torsions, are introduced. We have chosen an harmonic

potential that forces the unit normal to the plane (C_1, C_2, C_1') to oscillate around its equilibrium position. This equilibrium position forms an angle of 35.04° with the direction which would have pointed toward the H atom bonded to C_2 if the latter were explicitly simulated. In the all atom model, the new bending interactions introduced by the H atom bonded to C_2 perform the same function and no ad hoc improper torsion potential is required.

The SHAKE algorithm[28] was used to constrain the covalent bonds to fixed lengths, as remarked in the Introduction. The motion of the phenyl group, represented as a planar, rigid collection of six carbons (and six hydrogens), was simulated by means of the algorithm described by Cicccotti et al.[19,20] The position and orientation of the phenyl group are then fully described when the positions $\mathbf{r}_3$, $\mathbf{r}_4$, and $\mathbf{r}_5$ of the three C atoms forming an equilateral triangle (see Figure 1) are known. The remaining three carbon atoms are then given in terms of $\mathbf{r}_3$, $\mathbf{r}_4$, and $\mathbf{r}_5$ by

$$\mathbf{r}_i = {}^2/_3(\mathbf{r}_3 + \mathbf{r}_4 + \mathbf{r}_5) - \mathbf{r}_{i-3} \qquad (i = 6, 7, 8) \qquad (1)$$

In the united atom model, the forces acting on atoms 6, 7, and 8 are transmitted to atoms 3, 4, and 5 by virtue of the constraints expressed by eq 1, and the effective equations of motion for the latter three atoms become

$$(m_0 + m_1)\, \mathrm{d}^2\mathbf{r}_3/\mathrm{d}t^2 = \mathbf{F}_3 + \mathbf{G}_3 \qquad (2)$$

$$2m_1\, \mathrm{d}^2\mathbf{r}_4/\mathrm{d}t^2 = \mathbf{F}_4 + \mathbf{G}_4 \qquad (3)$$

$$2m_1\, \mathrm{d}^2\mathbf{r}_5/\mathrm{d}t^2 = \mathbf{F}_5 + \mathbf{G}_5 \qquad (4)$$

where m_0 is the mass of a carbon atom, m_1 is the combined mass of a carbon and a hydrogen atom, $\mathbf{F}_3$, $\mathbf{F}_4$ and $\mathbf{F}_5$ are the effective forces acting on atoms 3, 4, and 5, respectively, and $\mathbf{G}_3$, $\mathbf{G}_4$, and $\mathbf{G}_5$ are the constraint forces required to keep the bond length between atoms 2 and 3 and the distances among atoms 3, 4, and 5 constant. The effective forces $\mathbf{F}_3$, $\mathbf{F}_4$, and $\mathbf{F}_5$ are given by

$$\mathbf{F}_i = \mathbf{f}_i - \mathbf{f}_{i+3} + {}^2/_3(\mathbf{f}_6 + \mathbf{f}_7 + \mathbf{f}_8) \qquad (i = 3, 4, 5) \qquad (5)$$

where $\mathbf{f}_i$ (i = 3–8) are the actual forces acting on the respective atoms. The constraint forces $\mathbf{G}_3$, $\mathbf{G}_4$, and $\mathbf{G}_5$ contain terms consisting of a product of a Lagrangian multiplier and the distance between a pair of atoms (among atoms 2–5) that is held fixed. In solving eqs 2–4, the effect of these constraint forces is taken account of by means of the SHAKE algorithm.[28]

In the case of the all atom model, eqs 2–4 still describe the motions of the carbon atoms C_3, C_4, and C_5, but the forces acting on the hydrogen atoms, in addition to those acting on C_6, C_7, and C_8, are now indirectly transmitted to and influence the motions of these three base atoms. We do not describe the full details of the implementation of the Ciccotti–Ferrario–Ryckaert algorithm to the all atom model but instead give a brief remark in the Appendix to point out a few salient points.

The starting configurations of the polystyrene chain packed to the basic MD cell in a realistic density were generated as follows. First, we produced a chain having 80 styrene monomeric units with its backbone carbons all in trans conformations. This stretched-out chain was placed in a cubic MD cell whose size was made sufficiently large to ensure that none of the atoms on this chain would overlap with any of the images generated by the periodic boundary conditions. The MD program was then run to allow the chain to relax, and at the same time the size of the MD cell was gradually reduced to the final desired value. During the initial phase of this relaxation process, the nonbonded interaction force employed was greatly weakened to reduce the chance of violent repulsion occurring between atoms that happen to come too close to each other. Preparing the starting configuration in this manner is a fairly simple, straightforward operation, which is also efficient and consumes only a small fraction of the total cpu time required in the study.

The Newtonian equation of motion was integrated by use of the Verlet algorithm[27] at a time step of 10 fs in the united atom model program. It was confirmed that the total momentum of the system was strictly conserved, so that the center of mass of the molecule did not move during the simulation. The fairly large time step chosen, together with the random fluctuation associated with the constraint forces, produced moderate fluctuations in the total energy. The extent of the fluctuation, measured during microcanonical runs, amounted to about 10% of the fluctuations in kinetic energy. Such fluctuations are expected to introduce a negligible effect to the static properties that are being considered in this work. This was also confirmed by a comparison with results obtained with a reduced time step (5 fs). In the all atom model program a time step of 2.5 fs was used. The need for this reduced time step arose essentially because of the reduced stability of the SHAKE routine when applied to the displacements of fast-moving aliphatic hydrogen atoms. On a Cray Y-MP an integration step took about 0.09 and 0.22 s in the united atom and all atom models, respectively. Thus for a run of 1-ps duration in real time 9 and 88 s of cpu time are required, respectively. Inclusion of hydrogens is thus seen to increase the computation time by an order of magnitude. They are to be compared also with the 1.2 s that is required for a 1-ps run with our polyethylene model having 500 united CH_2 atoms.[30–33] While the programs were tested in the microcanonical ensemble, the production runs were performed at constant temperature, using the particle velocities rescaling scheme of Berendsen et al.[34]

Results and Discussion

To examine the degree to which our model has succeeded in simulating the real amorphous polystyrene, we calculate the X-ray scattering intensity curves from the simulation result and compare them with experimental data. When the united atom model was used for simulation, the hydrogen atoms were added, before the X-ray scattering patterns were calculated, in the appropriate positions relative to those of the carbon atoms obtained in the simulation.

To extract information on the structure of the material from the X-ray scattering pattern, it is more useful to evaluate the so-called reduced intensity function (or interference function) defined by

$$I(q) = kI_{\mathrm{coh}}(q) - \sum x_i f_i^2(q) \qquad (6)$$

where $I_{\mathrm{coh}}(q)$ is the coherently scattered intensity obtained after corrections have been made to the raw intensity data for background, absorption, multiple scattering, incoherent scattering, etc., k is a normalization constant needed to place the intensity on an absolute scale (in electron units per atom), x_i is the atomic fraction of species i, and $f_i(q)$ is its atomic scattering factor. Subtracting the weighted

sum of $f_i^2(q)$ eliminates contributions to $I(q)$ by the atoms scattering independently of each other. For the purpose of deriving the atomic radial distribution function by Fourier transformation of the intensity function, $I(q)$ is further modified to give the *sharpened* reduced intensity function $i(q)$ defined by

$$i(q) = I(q)/[\sum x_i f_i(q)]^2 \quad (7)$$

From the knowledge of atomic coordinates the X-ray intensity, for isotropic materials, can be calculated by

$$I(q) = \frac{1}{N}\sum\sum f_m f_n \frac{\sin qr_{mn}}{qr_{mn}} \quad (8)$$

where N is the total number of atoms in the system, r_{mn} is the distance between atoms m and n, and the summations run over all the atoms in the system, except for the terms with $m = n$. Since only two species of atoms, C and H, are present in our system, eq (9) can be rewritten[35,36] in terms of the pair distribution functions $g_{CC}(r)$, $g_{HH}(r)$, and $g_{CH}(r)$ as follows:

$$I(q) = \langle\rho\rangle \int dr\, 4\pi r^2 \frac{\sin qr}{qr}[f_C^2 x_C^2\{g_{CC}(r) - 1\} + f_H^2 x_H^2\{g_{HH}(r) - 1\} + 2f_C f_H x_C x_H\{g_{CH}(r) - 1\}] \quad (9)$$

where $\langle\rho\rangle$ is the average (number) density of all atoms in the system, and x_C and x_H are the atomic fractions. The pair distribution function $g_{ij}(r)$ is given by

$$g_{ij}(r) = \rho_{ij}(r)/\langle\rho_j\rangle \quad (10)$$

where $\rho_{ij}(r)$ is the density of atom j at a distance r from an atom i, and $\langle\rho_j\rangle$ is the average density of atom j. In our simulation the bond lengths were all kept fixed, whereas in reality the bond lengths fluctuate around their equilibrium lengths. To allow for the broadening of the pair distribution functions due to such bond length fluctuations, $g_{CC}(r)$, $g_{HH}(r)$, and $g_{CH}(r)$ evaluated from the atomic coordinates were first convoluted with a Gaussian function (with σ equal to 0.04 Å) before they were used in eq 9. The upper limit of the integration in (9) was set to 18 Å.

For the purpose of calculating the X-ray intensity curves, the MD program was run from three separate, well-equilibrated, starting configurations. The tacticity sequences of the chain in configurations A and B were identical, but the latter was derived from the former by running the MD program through a series of temperature–volume states that included a state of very low density, thus permitting a complete refolding of the chain into a new, dense state. Configuration C was made with a chain having a different tacticity sequence generated by an idependent Bernoulli run. Starting from these three different configurations (each of which were well equilibrated beforehand), the united atom model MD program was run for 500 ps at constant temperature and volume. To allow as much chain motions as possible to take place, the run was made not at room temperature but at 500 K, which is well above the experimental $T_g \sim 100$ °C. The density of the system was, however, kept at 1.028 g/cm^3, close to the experimental room-temperature density. Some preliminary study showed that the static properties were mostly sensitive to the choice of density rather than temperature. During the MD runs, atomic configurations were recorded at every picosecond, and the X-ray intensity curve was evaluated as an average over the 500 configurations thus recorded.

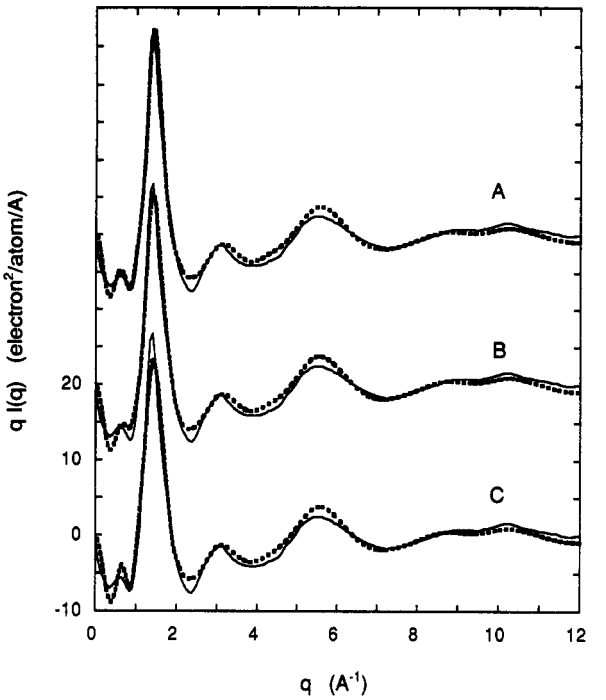

Figure 2. Plots of $qI(q)$ against q (=$4\pi \sin\theta/\lambda$), where $I(q)$ is the reduced intensity function defined by eq 6. The thick, broken curves give the results calculated from trajectories of 500-ps runs made with a unit atom model, starting from configuration A, B, or C, respectively. The thin solid curve is the observed data published by Mitchell and Windle.[16]

Figure 2 shows the X-ray intensity curves $qI(q)$ calculated with runs starting from the three starting configurations A, B, and C. To compare with experimental results, the data published by Mitchell and Windle[16] are superposed as thin solid lines. The Mitchell–Windle data are the most recent, and presumably the most accurate, of the several intensity data that were published in the past. (Since the data were taken from the published plot by scanning and digitization, some minor errors may have crept in in the process. Note also that the ordinate scale, unspecified in the original data, had to be arbitrarily adjusted to match our results.) It is seen that the polymerization peak at $q = 0.75$ A^{-1} is clearly reproduced with all three runs. The overall shape of the $qI(q)$ curves and the positions of all the peaks match well with those on the experimental curve, although some minor discrepancies in the intensity of the peaks and valleys are seen throughout. Whether one could expect an agreement much better than this, however, can be debated in view of the fact that experimental data themselves contain errors. The various corrections (especially for the incoherent scattering) that have to be applied to raw data to obtain $I(q)$ are known to be notoriously difficult. In Figure 3 the Mitchell–Windle data are compared with another curve published by Adams et al.[12] (which is in turn based on the earlier data by Wecker et al.[11]). Aside from the obvious slight mismatch in the q scale, one can also see discrepancies in the intensity to a degree that is comparable to the discrepancies seen in Figure 2. The mismatch in the shape of the polymerization peak is more pronounced, and this may in part reflect the fact that the polymerization peak is more sensitive to the temperature and to the thermal history of the sample.[37] It appears in any case that even if there might remain a need to improve our model further, the success of such attempts can no longer be judged on the basis of comparison with experimental X-ray intensity curves alone.

The radial distribution function can be obtained from the sharpened reduced intensity function $i(q)$ defined by

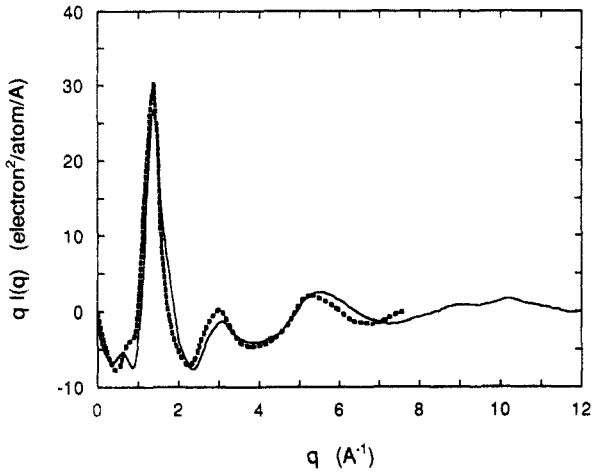

Figure 3. $qI(q)$ data published by Mitchell and Windle[16] compared with similar data by Adams et al.[12] which are based on measurement performed by Wecker et al.[11]

eq 7 by Fourier transformation:

$$4\pi r^2\Delta\rho(r) = (2r/\pi)\int_0^\infty qi(q)\sin(qr)\,dr \qquad (11)$$

where $\Delta\rho(r) = \rho(r) - \rho_0$ is the deviation from the average ρ_0 in the atomic density $\rho(r)$ at a distance r from an arbitrary atom. The radial distribution function $\rho(r)$ obtained by eq 11 is a weighted and smeared average[15,35] of the individual atomic pair distribution functions $\rho_{CC}(r)$, $\rho_{HH}(r)$, and $\rho_{CH}(r)$, because there are two types of atoms, C and H, present in the system and also because the q dependency of the atomic scattering factor for C is different from that for H. The individual, unsmeared, pair distribution functions can be readily evaluated directly from the MD results, as will be described later. At this point, however, we calculate the X-ray-smeared radial distribution function $\rho(r)$, for the purpose of comparing with experimental radial distribution functions, by following a procedure exactly the same as is used in the analysis of experimental data. In eq 11 the upper integration limit extends to infinity, whereas an experimental $i(q)$ is available only up to an upper limit q_{max} dictated by experimental conditions. Such a truncation of integration beyond q_{max} is known to introduce spurious subsidiary oscillations in the derived radiation distribution function. To minimize the truncation error it is customary to multiply the $i(q)$ by a smoothing function $M(q)$ before the integration:

$$4\pi r^2\Delta\rho(r) = (2r/\pi)\int_0^\infty qi(q)\,M(q)\sin(qr)\,dr \qquad (12)$$

An example of the smoothing function $M(q)$, employed by Schubach et al.[17] in their study of polystyrene radial distribution function, is given by

$$M(q) = \frac{\sin(\pi q/q_{max})}{\pi q/q_{max}} \qquad q \le q_{max}$$
$$= 0 \qquad q > q_{max} \qquad (13)$$

Figure 4 gives the results of applying eq 12 to the intensity functions shown in Figure 2. The thin solid lines give the most recent experimental result, the one obtained by Schubach et al. (Not sufficient information is available in their paper[17] to allow conversion of their ordinate scale to ours, and therefore it was arbitrarily adjusted to match our results.) In both calculations q_{max} is equal to 8 Å^{-1} and the smoothing function $M(q)$ defined by eq 13 is used.

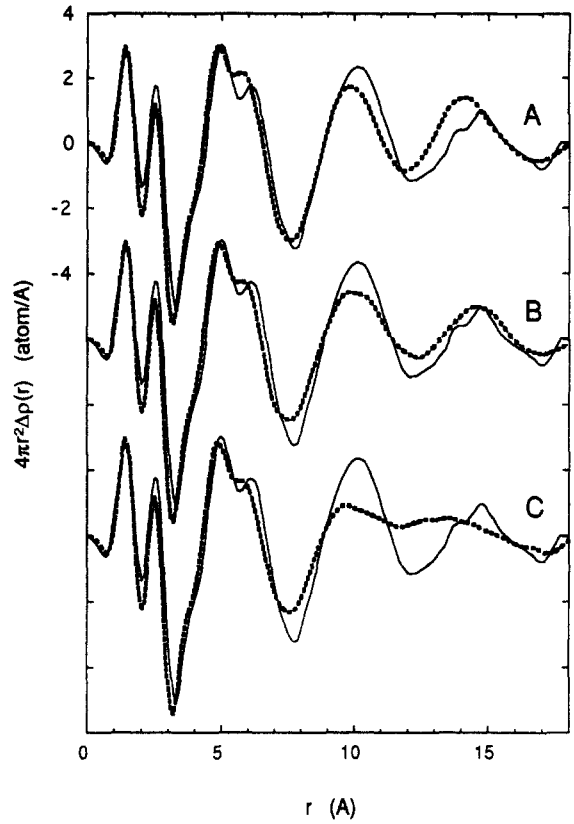

Figure 4. Radial distribution functions derived from Fourier transform of the corresponding intensity functions A, B, and C shown in Figure 2. The thin solid curve is the radial distribution function determined by Schubach et al.[17] from their X-ray measurement.

There is a fairly good agreement between the experiment and calculation for r up to about 9 Å, in regard to both the positions and shapes of the peaks, although some mismatch in the height of peak and depth of valley is apparent. The short-range correlations below about 5 Å arise mostly from the dispositions of atoms constrained by bond lengths and bond angles, which are known with a fair degree of certainty, and it is therefore not surprising to see a rather good agreement in this range. For r larger than 10 Å, the agreement is less satisfactory, although the overall shape of the curve is still fairly well reproduced, especially with configurations A and B. It is surprising that the apparently minor differences in the shape of the scattering curves among the three configurations, seen in Figure 2, cause such large differences in the radial distribution function at large r seen in Figure 4.

To see how reproducible the experimental radial distribution functions are when obtained in different laboratories, the intensity data by Mitchell and Windle, shown in Figures 2 and 3, were subjected to the same Fourier transform procedure, and the result is compared in Figure 5 with the one published by Schubach et al. Here again, we see that the difference between the two experimental functions is appreciable, and the extent of discrepancy is at least comparable to the deviation of our calculated radial distribution functions from the one by Schubach et al. The radial distribution function derived by Wecker et al.[11] differs even more markedly from either of the two curves in Figure 5.

In the calculated curves in Figure 4, fine details are absent beyond r = 10 Å, and only a large oscillation with a period of 4–5 Å remains, whereas in the both experimental curves in Figure 5 small modulations are seen to persist at large r. These small ripples are likely to be artifacts introduced by truncation and some other experimental

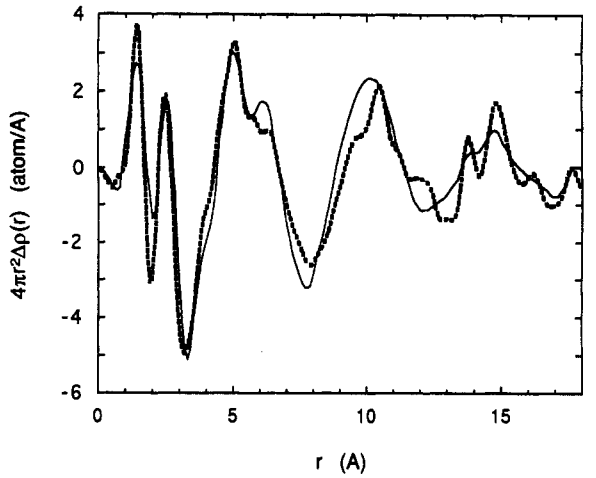

Figure 5. Radial distribution function published by Schubach et al.[7] (thin solid line) compared with the function obtained by Fourier transform of the intensity function by Mitchell and Windle[16] (thick broken line).

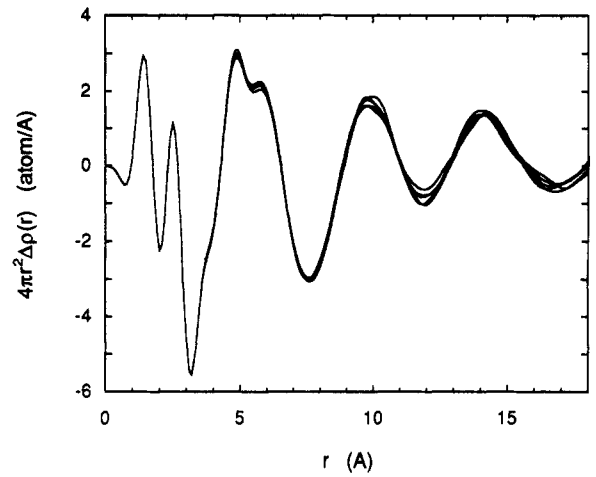

Figure 6. The 500-ps run starting from configuration A was broken up into a sequence of five segments of 100 ps each, and the RDP derived separately for each segment is plotted together here to show the changes in RDF that occur as the configuration of the polymer changes with time.

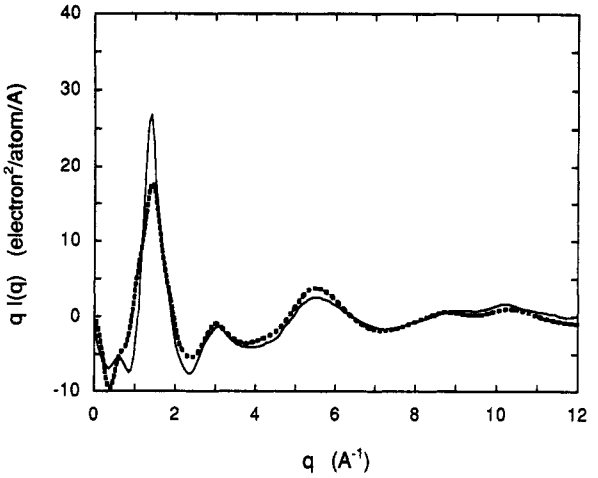

Figure 7. The X-ray intensity $qI(q)$ curve obtained from the all atom model (starting from configuration A) is shown here (thick broken line) and is seen to deviate appreciably from the Mitchell–Windle data[16] (thin solid line) for q smaller than about 2 Å^{-1}.

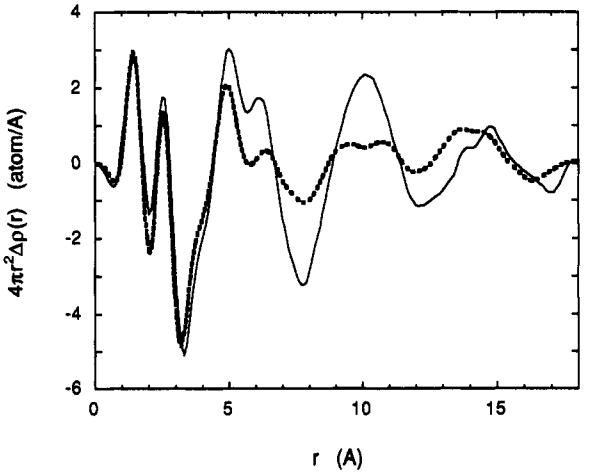

Figure 8. RDF (thick broken curve) calculated from the intensity curve in Figure 7, that was derived from MD simulation of the all atom model starting from configuration A, compared with the experimental RDF determined by Schubach et al.[17] (thin solid curve). The mismatch is appreciable for r greater than 5 Å.

errors. To see this, we have divided up the 500-ps run starting from configuration A into a sequence of 5 segments of 100 ps each and evaluated the RDF for each segment separately, which are plotted together in Figure 6. These five RDFs show clear differences in the long-range correlations beyond r about 9 Å. Averaging of many of these RDFs that accrue during a long MD run should smooth out all the fine details in the large r range. The same would be true with an experimental RDF which essentially corresponds to an average over time and also over an ensemble of many different configurations.

As mentioned earlier, we developed the all atom model program as a means of investigating any shortcomings of the united atom model that might arise as a result of the united atom approximation. It was to our great surprise that our all atom model gave curves, in both X-ray intensity and RDF, that showed much worse agreement with experiment. Figure 7 gives the $qI(q)$ curve obtained from a 200-ps run, which took its starting configuration from the configuration attained at the end of the 500-ps run A shown in Figures 2 and 4. Runs similarly based on configurations B and C give curves not very different from this one. They all deviate appreciably from the Mitchell–Windle data shown; the polymerization peak is all but obliterated, and the main amorphous peak is broader and less tall. In Figure 8 the RDF curve obtained in the same run is compared with the Schubach–Nagy–Heise data, and the agreement for r beyond 5 Å is very poor. To gain some idea of what change in structure has brought about the loss of the polymerization peak, the following exercise was performed. The inset in Figure 9 shows a portion of the scattering curve by Mitchell and Windle[16] (solid curve) and another one obtained from it by manually eliminating the polymerization peak (broken curve). The RDFs derived by Fourier transform from these two curves are shown in Figure 9. It is seen that the difference is not confined to any single atomic separation r but is spread over a wide r range centered around ca. 8 Å (=$2\pi/0.75$ Å^{-1}). It thus suggests that some long-range interactions involving nonbonded forces are apparently not correctly represented in our all atom force field, but we cannot say which of the parameters listed in Table 2 might be at fault. Incidentally, we also tried one of the widely available commercial molecular modeling programs to perform MD simulation of an all-atom, fully vibrational model of amorphous polystyrene. In this we took the built-in force-field parameters available in the program, which include electrostatic interactions due to partial charges residing on carbon and its associated hydrogen atoms. It gave a result that resembled the one obtained from our all atom model, but its agreement with experiment was even less satisfactory.

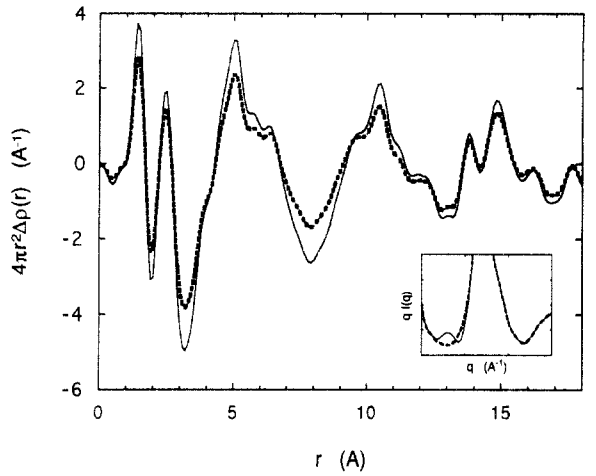

Figure 9. To understand the structural features that contribute to the polymerization peak, the scattering curve $qI(q)$ obtained by Mitchell and Windle was modified manually as shown in the inset. The RDF obtained by Fourier transform of the original Mitchell–Windle data (solid curve) is then compared with the RDF obtained from the modified scattering curve (broken curve).

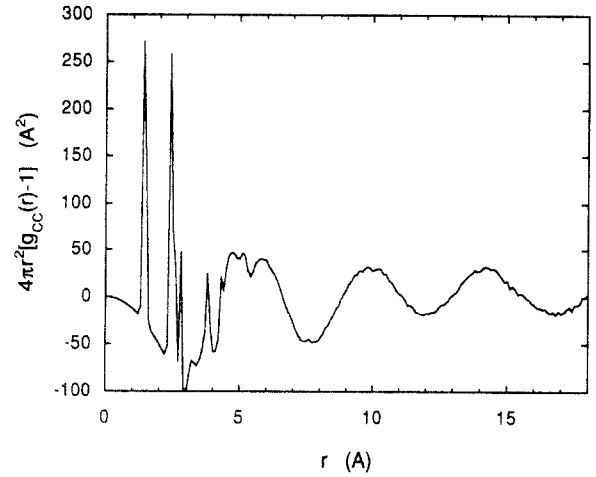

Figure 10. Atomic pair correlation function $g_{CC}(r)$ evaluated from the 500-ps run starting from configuration A.

As remarked earlier, the RDF derived from Fourier transformation of experimental intensity data is smeared. Now we examine the extent of such smearing. For this purpose we compare the RDF that can be obtained directly from the simulation result with the one that was obtained by first calculating the intensity function and then taking the Fourier transform of it. Figures 10–12 give the atomic pair distribution functions g_{CC}, g_{HH}, and g_{CH}, as defined in eq 10, that were derived from the trajectory of the 500-ps run starting from configuration A (and after the Gaussian broadening with $\sigma = 0.04$ Å was applied). In the case of g_{CC} one can clearly recognize five distinct peaks for r below 4 Å, but for r beyond 5 Å individual peaks are no longer recognizable because of overlap of interatomic pairs having closely similar separations and also because of the effect of averaging over configurations changing with time. The contributions of individual atomic pair correlation functions g_{CC}, g_{HH}, and g_{CH} to the intensity function are to be weighted, according to eq 9, by $f_C^2x_C^2$, $f_H^2x_H^2$, and $2f_Cf_Hx_Cx_H$, respectively. Because of the difference in q dependency between $f_C(q)$ and $f_H(q)$, these weighting factors change, in their relative magnitude, as q changes. In the hypothetical case where the ratio $f_C(q)/f_H(q)$ is fixed to the ratio Z_C/Z_H of the atomic numbers and remains constant, the Fourier transform of the intensity would give[38] a RDF related to g_{CC}, g_{HH}, and g_{CH} by

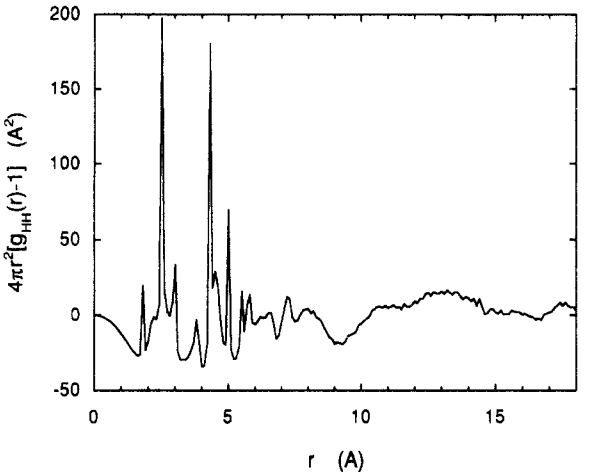

Figure 11. Same as Figure 10 but the pair correlation function is for H–H pairs.

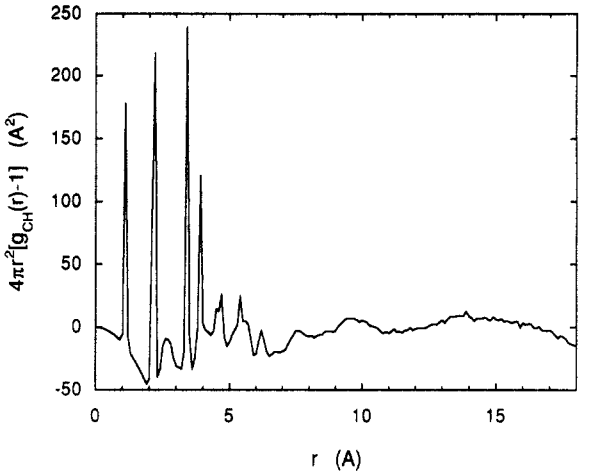

Figure 12. Same as Figure 10 but the pair correlation function is for C–H pairs.

$$\Delta\hat{\rho}(r) = \frac{\rho_0}{(Z_Cx_C + Z_Hx_H)^2}[Z_C^2x_C^2\{g_{CC}(r) - 1\} + Z_H^2x_H^2\{g_{HH}(r) - 1\} + 2Z_CZ_Hx_Cx_H\{g_{CH}(r) - 1\}] \quad (14)$$

The "desmeared" RDF $\Delta\hat{\rho}(r)$ evaluated according to eq 14 is plotted in Figure 13. Also shown in dotted line, for comparison, is the "smeared" RDF presented in Figure 4 as curve A. We see that among the two clearly recognizable peaks in the X-ray-smeared RDF, the first peak arises from an overlap of two peaks and the second peak from an overlap of three peaks. The comparison shows that the amount of structural information that can be obtained from the RDF based on X-ray measurement is severely limited by such a smearing effect.

The smearing arises partly because of the unequal q dependence of f_C and f_H but also because of the effect of multiplying the scattering intensity by the smoothing function $M(q)$ before Fourier transformation. The Fourier transform of $\sin(\pi q/q_{max})/(\pi q/q_{max})$ is equal to $(q_{max}/2\pi)$-$\Pi(rq_{max}/2\pi)$, where $\Pi(x)$ is a function[39] equal to 1 for $|x| \leq 1/2$ and equal to 0 for $|x| > 1/2$. Therefore the consequence of multiplying $i(q)$ with the smoothing function $M(q)$ defined in (13) before the integration is approximately equivalent to convoluting the RDF with $(q_{max}/2\pi)\Pi(rq_{max}/2\pi)$ after the Fourier transformation. When q_{max} is equal to 8 Å^{-1}, as is the case with most X-ray studies using Cu Kα radiation, the width of the $\Pi(rq_{max}/2\pi)$ function is approximately ±0.4 Å. The resolution of the RDF convoluted with $(q_{max}/2\pi)\Pi(rq_{max}/2\pi)$ is therefore limited

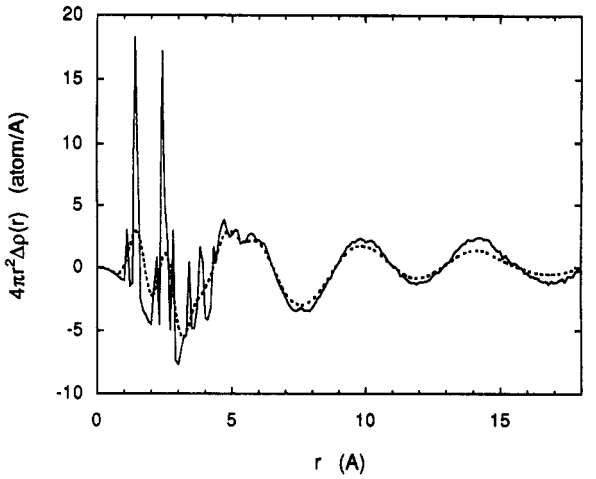

Figure 13. The solid curve is the "desmeared" radial distribution function $\Delta\hat{\rho}(r)$, which is the weighted average of the three pair distribution functions shown in Figures 10–12. The broken curve is the X-ray-smeared RDF (shown earlier in Figure 4 as curve A), which were obtained by using the same method of analysis as normally employed to process experimental X-ray intensity data.

at most to about ±0.4 Å, and this explains why the sharp peaks in the lower r region in Figure 13 are severely smeared. At larger r, the peaks in $\Delta\hat{\rho}(r)$ are already smeared due to the overlap of many different pair distances, even without the additional smearing due to the smoothing function. If, on the other hand, a smoothing function is not used at all in (12) and the integration is simply truncated beyond an upper limit q_{max}, the effect is the same as having multiplied $i(q)$ with a smoothing function $M(q) = \Pi(q/2q_{max})$. The Fourier transform of the latter is $\sin(rq_{max})/(\pi r)$, which has a main peak with a half-width at half-maximum roughly equal to $r = 0.6/q_{max}$ (or ca. 0.08 Å when $q_{max} = 8$ Å^{-1}) and many subsidiary oscillations at larger r with ever diminishing amplitudes. The RDF obtained without a smoothing function is equivalent to the convolution product of the true RDF with $\sin(rq_{max})/(\pi r)$, and therefore its sharp peaks at low r are smeared to a much lesser degree. On the other hand, the slow oscillations at higher r are modulated with many smaller spurious peaks. It appears therefore that the use of a smoothing function in the Fourier transform is useful for the study of features in the RDF occurring at higher r, but the features in the RDF at lower r are relatively better resolved when a smoothing function is not used at all.

Summary

The short-range order in amorphous polystyrene, i.e., the way atoms and segments are packed in the vicinity of each other to produce the dense glassy structure, has been the subject of interest by many since almost the inception of polymer science. Over the years more X-ray scattering studies have been performed on polystyrene than on any other amorphous polymer. The technique of molecular dynamics simulation, which has now become widely available for the study of polymers, has been applied in this work to this long-standing problem. We apply the MD technique to two models of atactic polystyrene, a united atom model and an all atom model. In both models the bond lengths are held fixed, and the phenyl group is constrained to be a rigid, planar hexagon. The SHAKE algorithm[28] and the constrained geometry algorithm of Ciccotti et al.[19] were used. The basic MD cell contained an atactic chain consisting of 80 styrene monomer units. The computational speed of the united atom model was found to be about an order of magnitude greater than the all atom model. The purpose of studying the all atom model was to see the extent of approximation that might be introduced in the united atom model at the price of computational efficiency. To our surprise, the all atom model produced results much worse than the united atom model for a reason that is not understood at this time.

The degree to which our models succeeded in simulating the real polymer was tested by calculating an X-ray scattering intensity curve and comparing it with experimental curves. The MD programs were run for three different chain configurations, the first two having the same stereochemical sequences and the third having an entirely different sequence. The $qI(q)$ curves calculated with the united atom model program agree fairly well with the experimental data published by Mitchell and Windle.[16] The positions and shapes of the peaks, including the so-called "polymerization peak", agree well, while there are some minor differences in the heights of the peaks. The results derived from the three starting configurations differ from each other to a minor extent. The degree of mismatch between simulation and experiment is, moreover, comparable to the degree of discrepancy between published experimental curves obtained by different groups of workers. It suggests that if there exists any need to further improve our model, such an effort cannot be guided by trying to achieve a better agreement with experimental X-ray intensity curves.

As a further means of testing our simulation results against experiment, we computed the atomic radial distribution function $\Delta\rho(r)$ from the intensity curve by following a Fourier transform procedure in exactly the same way as it was applied to the analysis of experimental data. The RDFs obtained with the united atom model program give a good agreement with the experimental curve published by Schubach et al.[17] for the range of r less than about 9 Å but the agreement at larger r (>10 Å) was only moderate. When two experimentally determined RDFs were compared, their agreement with each other were worse, again suggesting that existing X-ray data are not accurate enough to provide a guide for improving simulation models.

When the all atom model program was used, the results obtained were clearly inferior, showing that the calculated $qI(q)$ curve deviates clearly from the experimental one in the low q range (<2 Å^{-1}) and the calculated RDF fails to reproduce even the overall trend in the region of r larger than about 5 Å. We also tried one of the commercial software programs to build an all atom, fully vibrational model of atactic polystyrene with a force field that includes electrostatic interactions due to partial atomic charges, but the result was even worse than the one obtained with our own all atom model.

The RDF derived from Fourier transform of X-ray intensities is smeared because of the difference in the q dependence of the X-ray atomic scattering factors for C and H atoms and because of the limited q range available for experimental measurement. We evaluated the atomic RDF $\Delta\hat{\rho}(r)$, which is unmodified by such smearing, by analyzing the atomic coordinates obtained from the simulation. The result illustrates the extremely large effect of such smearing and the rather limited amount of information that can be derived from the experimental RDF. From examination of the calculated RDF and the changes that occur to it as the polymer molecule moves with time in the simulation, it can also be inferred that much of the fine details exhibited in the experimental RDF are artifacts due to erroneous processing of experimental intensity data.

Acknowledgment. This work was supported in part by the NSF Grant DMR8909232. The computation performed in this work was carried on the Cray Y-MP864 at the Ohio Supercomputer Center, and the generous allocation of cpu time is greatly appreciated.

Appendix

We here give a brief comment on the implementation of the constrained geometry algorithm of Ciccotti et al.[19,20] (CFR) and the use of the SHAKE routine in association with it.

The CFR algorithm deals with the case where the positions of secondary atoms can be fully expressed as linear combinations of the position vectors $\mathbf{R}_i$ of the base atoms. The equation of motion of the base atom can be written, in its most general form, as (see eq 11 of CFR)

$$\ddot{\mathbf{R}}_i = \sum_\alpha D_{i\alpha}\mathbf{f}_\alpha + \sum_j G_{ij}\mathbf{F}_j \qquad (15)$$

where $D_{i\alpha}$ and G_{ij} are time-independent constants with the dimensions of an inverse mass, and $\mathbf{f}_\alpha$ and $\mathbf{F}_j$ are the potential forces acting on the secondary and base atoms, respectively. In (15) we have ignored the constraint forces coming from the bond-length constraints on the base atoms, since these constraints will be enforced using the SHAKE method. In the united atom representation of the phenyl ring, there are three base atoms and three secondary atoms so that $D_{i\alpha}$ and G_{ij} are three by three matrices. In this particular case G_{ij} is in fact diagonal:

$$[G_{ii}] = \left[\frac{1}{m_0 + m_1}, \frac{1}{2m_1}, \frac{1}{2m_1}\right]$$

On the other hand, in the all atom representation of the phenyl ring, we have eight secondary atoms (three C and five H), so that $D_{i\alpha}$ is a three by eight matrix, and the off-diagonal elements of G_{ij} are also different from zero.

With regard to the application of the SHAKE routine, we should note that eq 15 is the result of a geometric construction (eq 6 of CFR) which applies irrespective of the character of the forces involved. In particular, it applies to constraint forces such as the ones introduced in the SHAKE method for bond-length constraints. In the SHAKE method, we apply recursively constraint-restoring forces to each pair of atoms connected by a bond. At each stage of the recursive process, the chosen magnitude of the force (equal for the two atoms) is, to some extent, a matter of convenience (although the final value is of course uniquely determined by the constrained equations of motion), but the force should always be directed along the original (unmoved) bond, in opposite directions for the two atoms. Ordinarily, therefore, this means that the acceleration and the induced restoring displacement of the two atoms along the bond will be inversely proportional to their masses. When we apply the SHAKE routine in combination with the geometric construction described in CFR, only the base atoms require adjustment, but we can no longer assume that the restoring displacement of an atom is simply proportional to the constraint force applied to it, since the rigid constraints introduced by the geometric construction require, in general, a transfer of force among the base atoms as well as between the secondary and the base atoms. That is, the off-diagonal elements of G_{ij} are, in general, different from zero, as is the case with our all atom representation of the phenyl ring. Even in the special case where G_{ij} is diagonal (as in the united atom representation of the phenyl ring), the element G_{ij} does not, in general, coincide with the inverse mass of the ith base particle (see above), and the magnitude of the restoring displacement is therefore affected.

References and Notes

(1) *Computer Simulation of Polymers*; Roe, R. J., Ed.; Prentice Hall: Englewood Cliffs, NJ, 1991.
(2) *Computational Modeling of Polymers*; Bicerano, J., Ed.; Marcel Dekker: New York, 1992.
(3) Allen, M. P., Tildesley, D. J. *Computer Simulation of Liquids*; Clarendon Press: Oxford, 1987.
(4) Khare, R.; Paulaitis, M. E.; Lustig, S. R. *Macromolecules* **1993**, *26*, 7203.
(5) Rapold, R.; Suter, U. W.; Theodorou, D. N. *Makromol. Chem. Theory Simul.* **1994**, *3*, 19.
(6) Katz, J. R.; Selman, J.; Heyne, L. *Z. Kautschuk* **1927**, 217.
(7) Katz, J. R. *Trans. Faraday Soc.* **1936**, *32*, 77.
(8) Krimm, S. *J. Phys. Chem.* **1953**, *57*, 22.
(9) Bjørnhaug, A.; Ellefsen, Ø.; Tønnesen, B. A. *J. Polym. Sci.* **1954**, *12*, 621.
(10) Kilian, G. G.; Bourke, K. *J. Polym. Sci.* **1962**, *58*, 311.
(11) Wecker, S. M.; Davidson, T.; Cohen, J. B. *J. Mater. Sci.* **1972**, *7*, 1249.
(12) Adams, R.; Balyuzi, H. H.; Burge, R. E. *J. Mater. Sci.* **1978**, *13*, 391.
(13) May, M. *J. Polym. Sci.: Polym. Symp.* **1977**, *58*, 23.
(14) Lovell, R.; Windle, A. H. *Polymer* **1976**, *17*, 488.
(15) Lovell, R.; Mitchell, G. R.; Windle, A. H. *Faraday Discuss.* **1979**, *68*, 46.
(16) Mitchell, G. R.; Windle, A. H. *Polymer* **1984**, *25*, 906.
(17) Schubach, H. R.; Nagy, E.; Heise, B. *Colloid Polym. Sci.* **1982**, *259*, 789.
(18) van Gunsteren, W. F.; Karplus, M. *Macromolecules* **1982**, *15*, 1528.
(19) Ciccotti, G.; Ferrario, M.; Ryckaert, J.-P. *Mol. Phys.* **1982**, *47*, 1253.
(20) Ciccotti, G.; Ryckaert, J. P. *Comput. Phys. Rep.* **1986**, *4*, 345.
(21) Claessens, M.; Ferrario, M.; Ryckaert, J.-P. *Mol. Phys.* **1983**, *50*, 217.
(22) Johnson, L. F.; Heatley, F.; Bovey, F. A. *Macromolecules* **1970**, *3*, 175.
(23) Weiner, S. J.; Kollman, P. A.; Case, D. A.; Singh, U. C.; Chio, C.; Alagona, G.; Profeta, S. Jr.; Weiner, P. *J. Am. Chem. Soc.* **1984**, *106*, 765.
(24) Weiner, S. J.; Kollman, P. A.; Nguyen, D. T.; Case, D. A. *J. Comput. Chem.* **1986**, *7*, 230.
(25) Abe, Y.; Tonelli, A. E.; Flory, P. J. *Macromolecules* **1970**, *3*, 294.
(26) Tonelli, A. E. *Macromolecules* **1973**, *6*, 683.
(27) Yoon, D. Y.; Sundararajan, P. R.; Flory, P. J. *Macromolecules* **1975**, *8*, 776.
(28) Ryckaert, J. P.; Ciccotti, G.; Berendsen, J. J. C. *J. Comput. Phys.* **1977**, *23*, 327.
(29) Verlet, L. *Phys. Rev.* **1967**, *159*, 98.
(30) Rigby, D.; Roe, R. J. *J. Chem. Phys.* **1987**, *87*, 7285; *Ibid.* **1988**, *89*, 5280.
(31) Rigby, D.; Roe, R. J. *Macromolecules* **1989**, *22*, 2259; *Ibid.* **1990**, *23*, 5312.
(32) Takeuchi, H.; Roe, R. J. *J. Chem. Phys.* **1991**, *94*, 7446, 7458.
(33) Roe, R. J.; Rigby, D.; Furuya, H.; Takeuchi, H. *Comput. Polym. Sci.* **1992**, *2*, 32.
(34) Berendsen, H. J. C.; Postma, J. P. M.; Van Gunsteren, W. F.; DiNola, A.; Haak, J. R. *J. Chem. Phys.* **1984**, *82*, 3684.
(35) Warren, B. E. *X-ray Diffraction*; Addison-Wesley: Reading, MA, 1969.
(36) Pings, C. J.; Waser, J. *J. Chem. Phys.* **1968**, *48*, 3016.
(37) Song, H. H.; Roe, R. J. *Macromolecules* **1987**, *20*, 2723.
(38) Wignall, G. D.; Longman, G. W. *J. Mater. Sci.* **1973**, *8*, 1439.
(39) Bracewell, R. N. *The Fourier Transform and Its Applications*, 2nd ed.; McGraw-Hill: New York, 1978.